Journal of Alloys and Compounds 677 (2016) 288–293

Contents lists available at ScienceDirect

Journal of Alloys and Compounds

journal homepage: http://www.elsevier.com/locate/jalcom

PVP assisted hydrothermal fabrication and morphology-controllable fabrication of $BiFeO_3$ uniform nanostructures with enhanced photocatalytic activities

Xingfu Wang [a, b], Weiwei Mao [a, b], Qiaoxia Zhang [a], Qi Wang [a], Yiyi Zhu [a], Jian Zhang [a], Tao Yang [a], Jianping Yang [b], Xing'ao Li [a, *], Wei Huang [a, c, **]

[a] Key Laboratory for Organic Electronics & Information Displays (KLOEID), Synergetic Innovation Center for Organic Electronics and Information Displays (SICOEID), Institute of Advanced Materials (IAM), School of Materials Science and Engineering (SMSE), Nanjing University of Posts and Telecommunications (NUPT), Nanjing 210023, PR China

[b] School of Science, Advanced Energy Technology Center, Nanjing University of Posts and Telecommunications (NUPT), Nanjing 210023, PR China

[c] Key Laboratory of Flexible Electronics (KLOFE), Institute of Advanced Materials (IAM), National Synergistic Innovation Center for Advanced Materials (SICAM), Nanjing Tech University (NanjingTech), 30 South Puzhu Road, Nanjing 211816, PR China

ARTICLE INFO

Article history:
Received 10 December 2015
Received in revised form
20 February 2016
Accepted 29 February 2016
Available online 31 March 2016

Keywords:
Morphology controllable
$BiFeO_3$
Nanostructures
Photocatalysis

ABSTRACT

Bismuth ferrite ($BiFeO_3$) nanostructures with various morphologies (spindles, cubes and plates) have been successfully synthesized via a convenient one-pot hydrothermal method. The results show that three kinds of $BiFeO_3$ products were obtained in this polyvinylpyrrolidone (PVP)-assisted hydrothermal reaction under different alkaline conditions. The resulting nanostructures were characterized using XRD and SEM. Possible formation mechanism for $BiFeO_3$ nanostructures was proposed on the basis of our results. The experiments showed that the visible light absorptive capacity of the $BiFeO_3$ nanostructures was significant influenced on the size and morphology. Notably, the as-prepared $BiFeO_3$ plates with (104) facets exposed exhibit high efficiency for the degradation of methyl orange (MO) under visible light irradiation, suggesting potential applications in photocatalytic and related areas under visible light.

© 2016 Elsevier B.V. All rights reserved.

1. Introduction

Perovskite ferroelectric oxides have attracted much attention over the past decade due to their fascinating physical properties and potential in applications [1–3]. As a typical multiferroic material [4–6], perovskite-type bismuth ferrite ($BiFeO_3$), with simultaneous ferroelectric and ferromagnetic ordering at room temperature, has attracted great attention due to its suitable band gap (~2.2 eV) and excellent chemical stability [7,8]. Morphology control for achieving preferential exposure of reactive crystal facets has received extensive attention [9,10]. The latest investigations on crystal facet engineering of semiconductors have demonstrated that photogenerated charge transfer to distinct crystal facets is closely related to their corresponding geometric and electronic properties [11]. Therefore, control of the shape and size of $BiFeO_3$ nanoparticles plays very important roles in determining magnetic, electrical, optical and catalytical properties due to the spatial geometry effect [12,13].

It is well known that phase pure $BiFeO_3$ is very difficult to synthesize because several impurity phases ($Bi_2Fe_4O_9$, $Bi_{25}FeO_{40}$ et al.) are often present, which would affect the electrical and magnetic properties of the overall material [14]. Relatively, the hydrothermal approach is a convenient route to fabrication the nanostructures [15–17]. Moreover, several reaction conditions, such as the mineralizer and the surfactant, can be employed to adjust the crystal nucleation and growth. In recent years, Fei et al. have successfully synthesized perovskite $BiFeO_3$ crystallites with different predominantly exposed facets *via* a facile one-pot hydrothermal approach under the presence of potassium hydroxide (KOH) and polyethylene glycol (PEG) [18]. The phase-pure $BiFeO_3$ pills and rods with highly exposed {111}c facets show an obviously

* Corresponding author.
** Corresponding author. Key Laboratory for Organic Electronics & Information Displays (KLOEID), Synergetic Innovation Center for Organic Electronics and Information Displays (SICOEID), Institute of Advanced Materials (IAM), School of Materials Science and Engineering (SMSE), Nanjing University of Posts and Telecommunications (NUPT), Nanjing 210023, PR China.
E-mail addresses: lxahbmy@126.com (X. Li), iamwhuang@njupt.edu.cn (W. Huang).

http://dx.doi.org/10.1016/j.jallcom.2016.02.246
0925-8388/© 2016 Elsevier B.V. All rights reserved.

enhanced visible light response when compared with {100}c dominant $BiFeO_3$ cubes. Yang et al. have roposed another simple hydrothermal process to prepare single-crystal $BiFeO_3$ microplates, where the precursor ($C_6H_{10}BiNO_8$) acts both as reactant and as surface modifier in the formation of the $BiFeO_3$ microplates [19]. The dielectric constant of the $BiFeO_3$/poly-vinylidene fluoride (PVDF) film is much higher than the pure $BiFeO_3$ at room temperature. Besides, Zhang et al. have successfully prepared nanoparticles-assembled one-dimensional $BiFeO_3$ microrods *via* a mild polymer directed solvothermal route [20]. The obtained $BiFeO_3$ microrods exhibit smaller saturation magnetizations and larger coercive force than the nanoparticles.

In spite of some studies focus on the morphology control and characterization, it is necessary to fabricate different-shaped $BiFeO_3$ nanostructures from the view of their morphology and size-dependent physical and chemical properties and wide practical applications [21–23]. In this work, we find a simple and controllable one-pot hydrothermal approach to create well defined perovskite $BiFeO_3$ with different morphologies. An inexpensive organic stabilizer like polyvinylpyrrolidone (PVP) is used as a surfactant in the synthesis of $BiFeO_3$ nanostructures which can react at relatively low temperature [24]. A possible formation mechanism for $BiFeO_3$ nanostructures was also proposed. The as-prepared $BiFeO_3$ nanostructures were characterized by XRD, FE-SEM, HRTEM, FTIR and UV–vis spectra. The photocatalytic activity of the catalysts was evaluated by degrading methyl orange (MO) dye solution under visible light irradiation.

2. Experimental section

2.1. Fabrication of $BiFeO_3$ nanostructures

Bismuth nitrate ($Bi(NO_3)_3\cdot 5H_2O$) and ferric chloride hexahydrate ($FeCl_3\cdot 6H_2O$) were purchased from Guangdong Xilong Chemical Co., Ltd., P. R. China. Sodium hydroxide (NaOH), methyl orange (MO) and Polyvinylpyrrolidone K-30 (PVP) were obtained from Sinopharm Chemical Reagent Corp, P. R. China. All chemicals were used as received without further purification.

$BiFeO_3$ nanostructures were synthesized by a simple hydrothermal method. In a typical synthesis, $Bi(NO_3)_3\cdot 5H_2O$ (2.425 g) and $FeCl_3\cdot 6H_2O$ (1.352 g) in a stoichiometric ratio (1:1 in molar ratios) were mixed in acetone (50 mL, 99.8%) and sonicated for 30 min. Then deionized (D.I.) water (200 mL) and concentrated ammonia were added under vigorous stirring until the pH value of the solution reached 10–11. The sediment was centrifuged out and washed with D.I. water several times until the pH value was neutral. Next, the red co-precipitate was redispersed in D.I. water. Under vigorous stirring, a certain amount of PVP and NaOH (5 mL) were added into the suspension. Then, the solution was placed inside a stainless steel autoclave with a Teflon liner and heated at 180 °C for 72 h. After cooling down to room temperature, the precipitate was harvested by filtration, washed with D.I. water and absolute ethanol for three times, respectively, and dried at 80 °C for 2 h.

2.2. Characterization

The morphologies of $BiFeO_3$ nanostructures were observed via scanning electron microscopy (SEM, S-4800, Hitachi; accelerating voltage = 10 kV). The obtained samples were characterized by XRD on a Bruker D8 Advance x-ray powder diffractometer with Cu Kα radiation ($\lambda = 1.5418$ Å) in the 2θ range of 20°–60° with a step size of 0.002° and a scan speed of 0.5 s per step. The accelerating voltage and the applied current were 40 kV and 40 mA, respectively. High-resolution transmission electron microscopy (HRTEM) images were performed using a JEOL JEM-2100 instrument at the accelerating voltage of 200 kV. The fourier transforms infrared (FTIR) spectra were taken with a PerkinElmer Spectrum Two infrared spectrophotometer. The specific surface area was determined by V-Sorb 2800P (Gold APP Instruments Corporation, China) through the BET method. UV–vis absorption spectra were obtained using a PerkinElmer Lambda 35 spectrophotometer. The visible light ($\lambda > 420$ nm) was obtained using a 500 W Xe lamp with a 420 nm cutoff filter to completely remove any radiation below 420 nm.

2.3. Photocatalytic tests

The photocatalytic activities of $BiFeO_3$ nanostructures were evaluated by degradation of MO aqueous solution under visible light irradiation. A 500 W Xe lamp was used as the light source, and visible-light irradiation was realized by attaching a 420 nm cutoff filter. In a typical photocatalytic test, 50 mg catalyst was dispersed in 50 mL MO aqueous solution with a concentration of 5 mg L^{-1}. Prior to irradiation, the suspensions were magnetically stirred in the dark for 1 h to ensure the establishment of an adsorption-desorption equilibrium. Then, at selected time intervals, samples were collected and filtered to remove the photocatalyst particles by centrifugation. After that, the solution was analyzed using an ultraviolet–visible light spectrophotometer. A blank test was also carried out on an aqueous MO solution without photocatalyst under the same condition.

3. Results and discussion

3.1. Characterization of samples

As an important surfactant, PVP is usually used to control the morphologies of bismuth-containing nanomaterials [25]. SEM was performed to characterize the morphology of all $BiFeO_3$ samples. Fig. 1 shows SEM images of the as-synthesized $BiFeO_3$ nanostructures obtained with 0.5 M NaOH. It is well known that PVP is a nonionic surfactant and the amount of PVP could markedly affect the morphology of the final product [26,27]. When quite a few PVP (0.02 g) was introduced into the reaction system, a large amount of inhomogeneous $BiFeO_3$ products were synthesized, as shown in Fig. 1a. Fig. 1b–c shows the size of the $BiFeO_3$ decreased by increasing the amount of PVP. Interestingly, when the amount of PVP is further increased to 0.5 g, well-defined and uniform $BiFeO_3$ spindle-like nanostructures can be obtained, as shown in Fig. 1d. It can deduce that a suitable amount of PVP is crucial for the synthesis of $BiFeO_3$ nanostructures in our experiments.

Further investigations showed that the morphological and dimensional changes in the as-synthesized $BiFeO_3$ nanostructures strongly depend on the NaOH concentration. The amount of PVP is fixed 0.5 g according to the above results. When the concentration of NaOH is 0.5 M, the $BiFeO_3$ product shows pure spindle-like particles in a large scale with average length of about 200 nm and average width of about 100 nm, as depicted in Fig. 2a. Owing to consisting of large amounts of small particles ~50 nm, the surfaces of these spindles are quite rough, and the specific surface area would be increased. With further increase of the NaOH concentration to 2 M, a number of $BiFeO_3$ cubes with edge lengths ranging from 100 nm to 200 nm can be observed as shown in Fig. 2b. According to the symmetries of perovskite $BiFeO_3$ and other relevant works [28,29], all the surfaces of cubes can be ascribed to $\{100\}_c$ crystal faces. For 4 M, irregular plates with the length ranging from 200 nm to 500 nm, showed a hexagonal shape on its front surface as the outline showed, and the thickness was *ca.* 50 nm, as shown in Fig. 2c. More interestingly, one side of the hexagonal plates with different degrees of truncation at edges is concave, which resulted

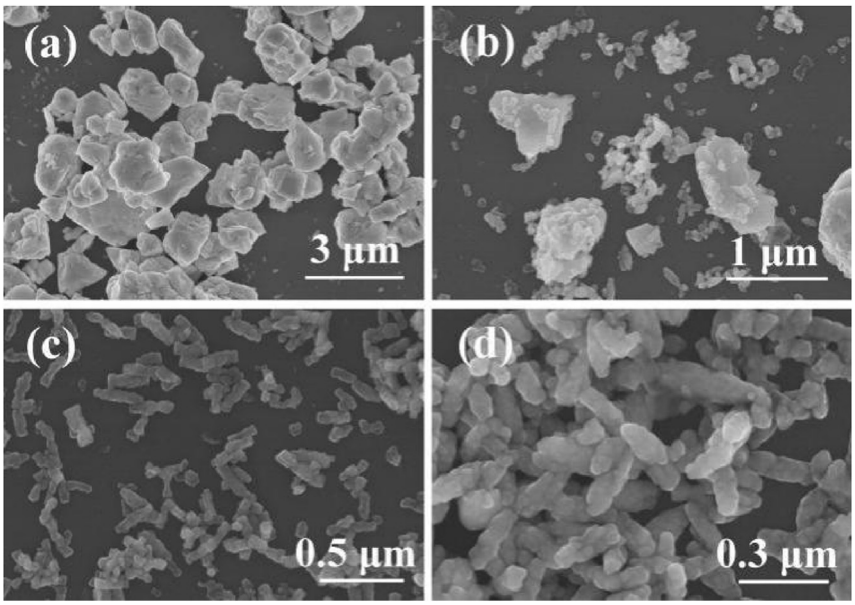

Fig. 1. SEM images of the $BiFeO_3$ nanostructures (0.5 M NaOH) obtained with various amount of PVP. (a) 0.02 g, (b) 0.1 g, (c) 0.2 g and (d) 0.5 g.

in exposing different facets. The surfaces of these $BiFeO_3$ plates are quite flat and the well-developed morphology suggests undoubted high crystallinity. The lateral thickness is less than 50 nm, which is much thinner, compared with the previously reported $BiFeO_3$ microplates dominated by (012) facets with the lateral length of 8 μm and a thickness of 510–550 nm [19]. Nanostructured materials have special physical and chemical properties, which is due to their anisotropic properties and a unique size effect.

The crystal phase of the materials is determined by XRD, as shown in Fig. 3. All the diffraction peaks can be indexed on the basis of a $BiFeO_3$ rhombohedral phase with the space group *R*3*c* (JCPDS card No. 86-1518). The intensity of the peaks for $BiFeO_3$ plates was clearly strengthened, which indicate that the sample is highly crystalline. As for the other two samples, a slight impurity phases (marked with "*") can be observed, and no secondary phase is observed. The inset of Fig. 3 is the enlarged version of the XRD patterns in the range of 2θ 31°–32.5°. It is worth noting that the (104) diffraction line of the $BiFeO_3$ plates intensified compared with the standard card, suggesting that the $BiFeO_3$ plates predominantly exposed the (104) facet. The results indicate that the diffraction peak intensity ratio of (104) to (110) crystal facets for the products can be delicately controlled by simply adjusting the addition amount of NaOH and PVP, suggesting that the anisotropic growth is perhaps preferential. The different exposed facets of all samples indicate that the products may have undergone a morphological evolution, which could lead to the difference in photocatalytic activity.

High-resolution transmission electron microscopy (HRTEM) was employed to analyze the crystalline structures of the $BiFeO_3$ samples and the images are shown in Fig. 4a–c. The rhombohedral structure of the $BiFeO_3$ spindles and cubes was confirmed by HRTEM analysis from the measured lattice distance of 3.96 Å along the (012) plane, as can be seen in Fig. 4a and b. From the HRTEM images, the observed lattice of the $BiFeO_3$ plates is 2.82 Å, which is consistent with the (104) crystal planes of a rhombohedral phase $BiFeO_3$ crystal (JCPDS No. 86-1518), as shown in Fig. 4c. Fig. 4d–f are the corresponding selected electron diffraction (SAED) pattern. The diffraction rings (Fig. 4d) are discontinuous and consist of sharp spots which indicate good crystallinity of $BiFeO_3$ spindles. The SAED pattern from an individual cube grain (Fig. 4e) shows very sharp diffraction spots, indicating the formation of well-developed single-crystalline $BiFeO_3$. The SAED pattern shows clear lattice planes, again confirming the pure crystallinity of the as-synthesized nanocrystals. Diffraction spots corresponding to the secondary and impurity phases were not present.

3.2. Optical and photocatalytic performance

Considering the potential optoelectronic applications of $BiFeO_3$ in photodetectors or solar cells, the optical properties of the as-prepared $BiFeO_3$ samples were investigated by UV–vis diffuse reflectance spectroscopy (DRS). As can be seen from Fig. 5, the broad absorption band indicated that all $BiFeO_3$ products can absorb considerable amounts of visible light, which suggest their potential applications as visible-light driven photocatalysts. It is well documented that the morphologies of semiconductors affect the light absorbance and band-gap energies [30]. Compared with that of spindles and cubes sample, the absorption edge of the plates distinctively broadened from visible to near-infrared region. Different from the three-dimensional materials ($BiFeO_3$ spindles and cubes), the electronic properties of two-dimensional materials are modulated in plane. Hence the photocatalyst of the plates could absorb more visible light to produce electron–hole pairs, which could be favorable for a photocatalytic reaction.

The FTIR spectra of the $BiFeO_3$ samples were studied, as shown in Fig. 6. The broad peak between 550 and 600 cm^{-1} in the FTIR spectrum is related to the Fe–O stretching and bending vibration of the octahedral FeO_6 groups in perovskite structures, which implying the formation of $BiFeO_3$ phase. The broad band at 3436 cm^{-1} (Fig. 6c) possibly arose from the antisymmetric and asymmetric stretching of H_2O and OH^- groups.

In contrast, therefore, we also investigated the catalytic activities of $BiFeO_3$ with various shapes. The photocatalytic performance of $BiFeO_3$ nanostructures was evaluated by the photodegradation of methyl orange (MO) aqueous solution under visible light irradiation after adsorption/desorption equilibration. The C/C_0 ratio graph is shown in Fig. 7. It was found that the $BiFeO_3$ cubes and the spindles degraded 38.7% and 49.8% of the dye, respectively, after 180 min radiation, while the plates degraded 69.1% of the dye under the same experiment condition. The specific surface area was

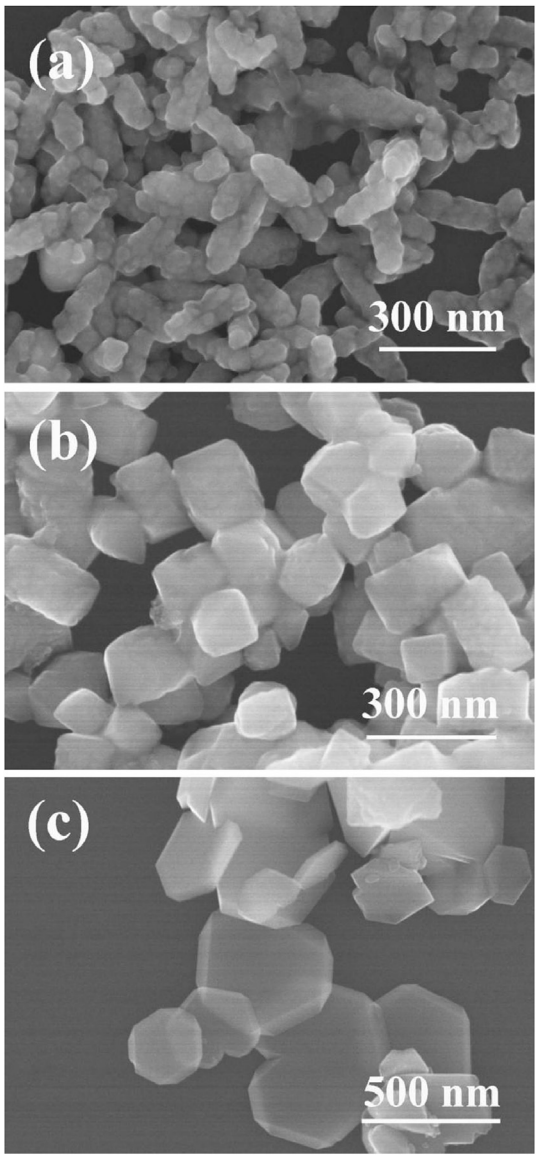

Fig. 2. SEM images of the $BiFeO_3$ nanostructures obtained with various concentration of NaOH: (a) 0.5 M, (b) 2 M and (c) 4 M.

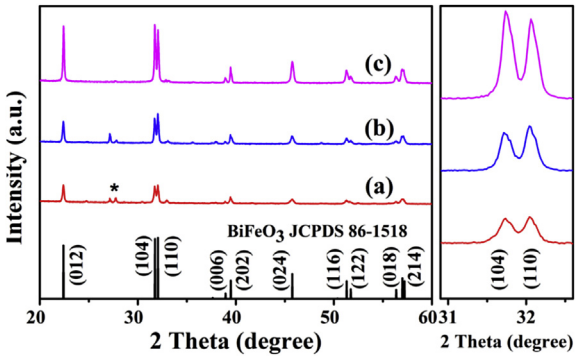

Fig. 3. XRD patterns of the $BiFeO_3$ samples: (a) spindles, (b) cubes and (c) plates.

obtained and the result showed that the specific surface area of spindles, cubes and plates is 0.874 m^2/g, 0.526 m^2/g and 0.766 m^2/g,

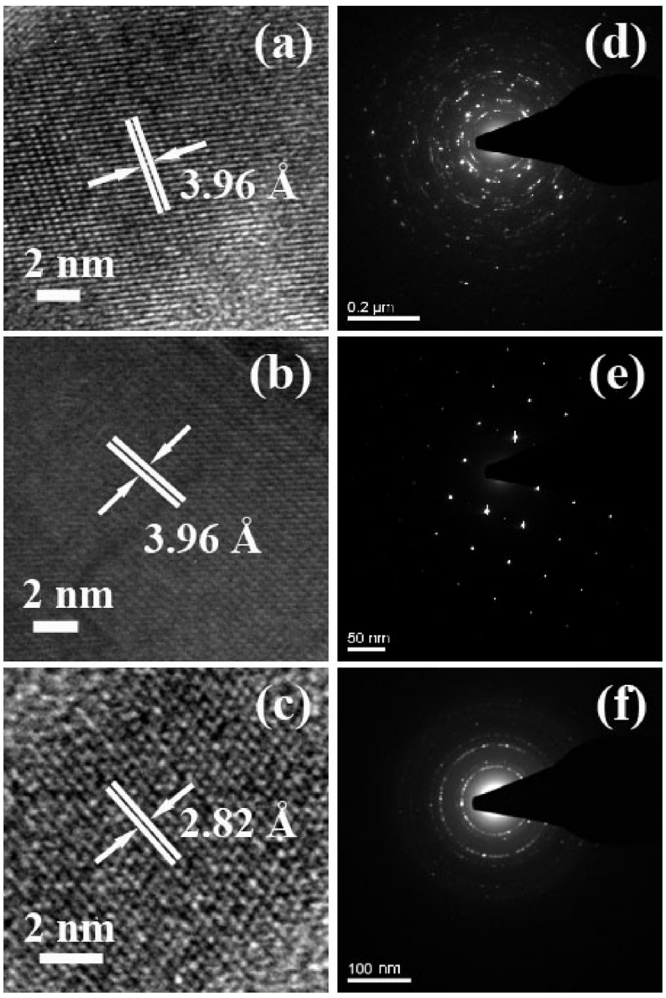

Fig. 4. HRTEM images of the $BiFeO_3$ samples: (a) spindles, (b) cubes and (c) plates, and corresponding SAED patterns: (d) spindles, (e) cubes and (f) plates.

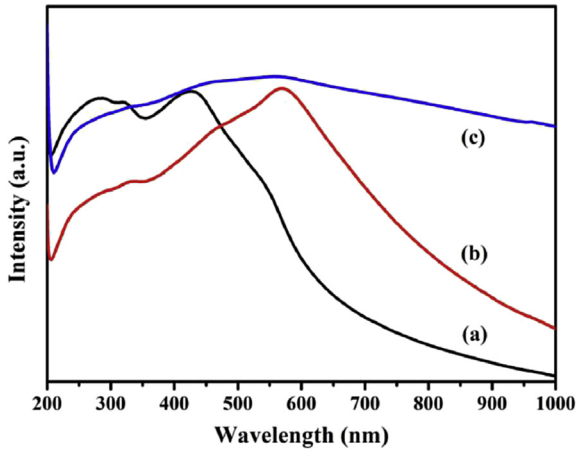

Fig. 5. UV–vis spectra of $BiFeO_3$ nanostructures: (a) spindles, (b) cubes and (c) plates.

respectively. Although the specific surface area of plates is not the maximum value among of them, the photocatalytic activity is the highest. The results showed that the optical properties of the $BiFeO_3$ nanostructures were strongly related to their shape and exposed facet. The possibility, which would enhance the catalytic

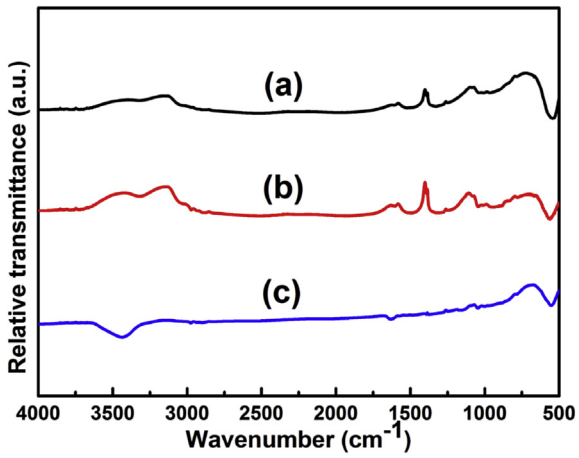

Fig. 6. FTIR spectrum of $BiFeO_3$ nanostructures: (a) spindles, (b) cubes and (c) plates.

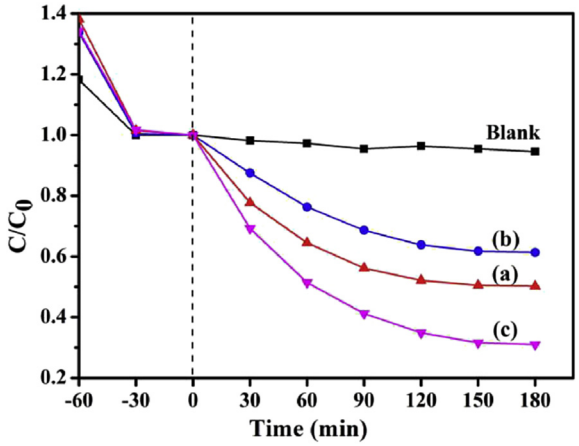

Fig. 7. Photocatalytic activity of different catalysts for the degradation of MO solution at room temperature: (a) spindles, (b) cubes and (c) plates.

activity in the plate structures, is excited photocatalytic species reaching to different exposed facets. Meanwhile, based on Fig. 3, it can be deduced that the exposed (104) facet was pivotal for achieving the high photocatalytic activity of the $BiFeO_3$ plates.

3.3. Growth mechanism

On the basis of the above results, a proposal formation mechanism of $BiFeO_3$ nanostructures is suggested as follows. The shape evolution of $BiFeO_3$ nanostructures are illustrated in detail in Fig. 8. Firstly, as we all know, $Bi(NO_3)_3$ hydrolyzed easily in water to produce slightly soluble irregular shaped $BiONO_3$ [31], while $Fe(OH)_3$ is resulted from the reaction between ferric chloride hexahydrate and ammonia. As a surface modifier, the PVP polymer could selectively absorb on the (012) and (104) facets of these nanoparticles due to its large number of carbonyl groups and amide ligands in the NaOH solution of various concentration. Bi ion combines easily with PVP by the chelating effect owing to the much higher stability constant than Fe ion. Then $BiFeO_3$ amorphous colloids are formed by a slow aggregation and crystallization of primary small seed particles [32,33]. Secondly, in the alkaline conditions, $BiFeO_3$ nanoparticles had a tendency to aggregate along a certain direction in order to minimize the overall energy of the reaction system. The alkaline concentration significantly influences the morphology of the products which has been discussed before. The preferential growth of the $BiFeO_3$ nanoparticles can be attributed to the different nanoparticle-aggregation potentials [34], leading to the anisotropic growth rates in different directions. For $BiFeO_3$ plates, $BiFeO_3$ nanoparticles aggregated along (104) direction more quickly than along (102) direction. The self-assembly and anisotropic growth process could be explained by the "oriented attachment" mechanism [35,36]. In the present work, PVP is not only as a surfactant, but also as the structure-directing reagent in the formation of $BiFeO_3$ nanostructures. The nuclei grew only along the directions unoccupied by PVP [37]. Compared with previous reports, it also indicates that the PVP is beneficial to reduce the size of products. Thirdly, the primary self-aggregate nanoparticles recrystallized according to the well-known Gibbs–Thomson law [38]. With the assistance of Ostwald ripening, the surface energy will be further decreased, thus the as-prepared $BiFeO_3$ nanostructures become much more stable [39].

4. Conclusions

In summary, we have successfully synthesized uniform $BiFeO_3$ nanostructures with tunable morphology via a facile PVP-assisted hydrothermal method under the presence of sodium hydroxide. The effect of the surfactant and alkaline concentration was investigated, indicating the role of these parameters to achieve controlled morphology. PVP is beneficial to not only reduce the size of products as a surfactant, but also control the direction of growth as the structure-directing reagent in the formation of $BiFeO_3$ nanostructures. The photocatalytic activity of the as-prepared $BiFeO_3$ plates with (104) facets exposed is the best among the three samples for methyl orange (MO) photodegradation under visible light irradiation. It is believed from the present work that the $BiFeO_3$ nanostructures are an economically viable perovskite oxide and a promising candidate with great potential for environment remediation application.

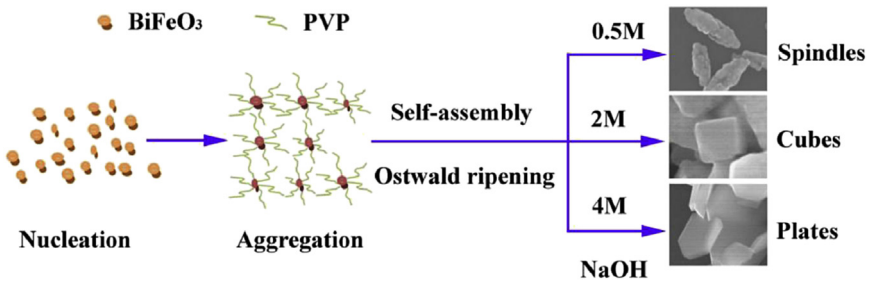

Fig. 8. Schematic illustration of the formation mechanism of $BiFeO_3$ nanostructures.

Acknowledgements

We acknowledge the financial support from the National Basic Research Program of China (2012CB933301, 2014CB648300), the Key Project of National High Technology Research of China (2011AA050526), the Ministry of Education of China (No. IRT1148), National Synergistic Innovation Center for Advanced Materials (SICAM), Natural Science Foundation of Jiangsu Province, China (BM2012010), the Project Funded by the Priority Academic Program Development of Jiangsu Higher Education Institutions (PAPD, YX03001), the National Natural Science Foundation of China (51172110, 51372119, 61377019, 61136003, 51173081), College Postgraduate Research and Innovation Project of Jiangsu Province (KYLX_0794, KYLX15_0848), the Natural Science Foundation of Nanjing University of Posts and Telecommunications (NY214129, NY214130, NY214181, NY215176).

References

[1] S. Farokhipoor, C. Magén, S. Venkatesan, J. Íñiguez, C.J.M. Daumont, D. Rubi, E. Snoeck, M. Mostovoy, C. de Graaf, A. Müller, M. Döblinger, C. Scheu, B. Noheda, Artificial chemical and magnetic structure at the domain walls of an epitaxial oxide, Nature 515 (2014) 379–383.
[2] K. Chu, B.K. Jang, J.H. Sung, Y.A. Shin, E.S. Lee, K. Song, J.H. Lee, C.S. Woo, S.J. Kim, S.Y. Choi, T.Y. Koo, Y.H. Kim, S.H. Oh, M.H. Jo, C.H. Yang, Enhancement of the anisotropic photocurrent in ferroelectric oxides by strain gradients, Nat. Nanotech. 10 (2015), 972–U196.
[3] Q.Q. Yang, H. Zhang, K.H. Linghu, X.G. Chen, J.B. Zhang, R.J. Nie, F.R. Wang, J.X. Deng, J.Y. Wang, The transport properties in $BiFeO_3$/YBCO heterostructures, J. Alloys Compd. 646 (2015) 1133–1138.
[4] S.V. Vijayasundaram, G. Suresh, R.A. Mondal, R. Kanagadurai, Substitution-driven enhanced magnetic and ferroelectric properties of $BiFeO_3$ nanoparticles, J. Alloys Compd. 658 (2016) 726–731.
[5] Y.M. Kim, A. Morozovska, E. Eliseev, M.P. Oxley, R. Mishra, S.M. Selbach, T. Grande, S.T. Pantelides, S.V. Kalinin, A.Y. Borisevich, Direct observation of ferroelectric field effect and vacancy-controlled screening at the $BiFeO_3$/$La_xSr_{1-x}MnO_3$ interface, Nat. Mater. 13 (2014) 1019–1025.
[6] W.W. Mao, X.F. Wang, Y.M. Han, X.A. Li, Y.T. Li, Y.F. Wang, Y.W. Ma, X.M. Feng, T. Yang, J.P. Yang, W. Huang, Effect of Ln (Ln = La, Pr) and Co co-doped on the magnetic and ferroelectric properties of $BiFeO_3$ nanoparticles, J. Alloys Compd. 584 (2014) 520–523.
[7] T.E. Quickel, L.T. Schelhas, R.A. Farrell, N. Petkov, V.H. Le, S.H. Tolbert, Mesoporous bismuth ferrite with amplified magnetoelectric coupling and electric field-induced ferrimagnetism, Nat. Commun. 6 (2015) 6562.
[8] Z.X. Li, Y. Shen, Y.H. Guan, Y.H. Hu, Y.H. Lin, C.W. Nan, Bandgap engineering and enhanced interface coupling of graphene–$BiFeO_3$ nanocomposites as efficient photocatalysts under visible light, J. Mater. Chem. A 2 (2014) 1967–1973.
[9] Y. Li, W.J. Shen, Morphology-dependent nanocatalysts: rod-shaped oxides, Chem. Soc. Rev. 43 (2014) 1543–1574.
[10] Q.Q. Shi, Y. Li, E.S. Zhan, N. Ta, W.J. Shen, Vanadia directed synthesis of anatase TiO_2 truncated bipyramids with preferential exposure of the reactive {001} facet, CrystEngComm 17 (2015) 3376–3382.
[11] G.G. Liu, T. Wang, W. Zhou, X.G. Meng, H.B. Zhang, H.M. Liu, T. Kako, J.H. Ye, Crystal-facet-dependent hot-electron transfer in plasmonic-Au/semiconductor heterostructures for efficient solar photocatalysis, J. Mater. Chem. C 3 (2015) 7538–7542.
[12] S. Godara, B. Kumar, Effect of Ba–Nb co-doping on the structural, dielectric, magnetic and ferroelectric properties of $BiFeO_3$ nanoparticles, Ceram. Int. 41 (2015) 6912–6919.
[13] I.T. Papadas, K.S. Subrahmanyam, M.G. Kanatzidis, G.S. Armatas, Templated assembly of $BiFeO_3$ nanocrystals into 3D mesoporous networks for catalytic applications, Nanoscale 7 (2015) 5737–5743.
[14] M. Hasana, M.F. Islama, R. Mahbuba, M.S. Hossainb, M.A. Hakim, A soft chemical route to the synthesis of $BiFeO_3$ nanoparticles with enhanced magnetization, Mater. Res. Bull. 73 (2016) 179–186.
[15] B. Sun, L.J. Wei, H.W. Li, P. Chen, White-light-controlled ferromagnetic and ferroelectric properties of multiferroic single crystalline $BiFeO_3$ nanoflowers at room temperature, J. Mater. Chem. C 2 (2014) 7547–7551.
[16] T. Fan, C.C. Chen, Z.H. Tang, Hydrothermal synthesis of novel $BiFeO_3$/$BiVO_4$ heterojunctions with enhanced photocatalytic activities under visible light irradiation, RSC Adv. 6 (2016) 9994–10000.
[17] J.P. Zhou, R.J. Xiao, Y.X. Zhang, Z.H. Shi, G.Q. Zhu, Novel behaviors of single-crystalline $BiFeO_3$ nanorods hydrothermally synthesized under magnetic field, J. Mater. Chem. C 3 (2015) 6924–6931.
[18] L.F. Fei, J.K. Yuan, Y.M. Hu, C.Z. Wu, J.L. Wang, Y. Wang, Visible light responsive perovskite $BiFeO_3$ pills and rods with dominant $\{111\}_c$ facets, Cryst. Growth Des. 11 (2011) 1049–1053.
[19] X. Yang, G. Xu, Z.H. Ren, X. Wei, C.Y. Chao, S.Y. Gong, G. Shen, G.R. Han, The hydrothermal synthesis and formation mechanism of single-crystalline perovskite $BiFeO_3$ microplates with dominant (012) facets, CrystEngComm 16 (2014) 4176–4182.
[20] L. Zhang, X.F. Cao, Y.L. Ma, X.T. Chen, Z.L. Xue, Polymer-directed synthesis and magnetic property of nanoparticles-assembled $BiFeO_3$ microrods, J. Solid State Chem. 183 (2010) 1761–1766.
[21] S. Li, J.M. Zhang, M.G. Kibria, Z. Mi, M. Chaker, D.L. Ma, R. Nechache, F. Rosei, Remarkably enhanced photocatalytic activity of laser ablated Au nanoparticle decorated $BiFeO_3$ nanowires under visible-light, Chem. Commun. 49 (2013) 5856–5858.
[22] X.F. Wang, W.W. Mao, J. Zhang, Y.M. Han, C.Y. Quan, Q.X. Zhang, T. Yang, J.P. Yang, X.A. Li, W. Huang, Facile fabrication of highly efficient g-C_3N_4/$BiFeO_3$ nanocomposites with enhanced visible light photocatalytic activities, J. Colloid Interface Sci. 448 (2015) 17–23.
[23] S. Mohan, B. Subramanian, A strategy to fabricate bismuth ferrite ($BiFeO_3$) nanotubes from electrospun nanofibers and their solar light-driven photocatalytic properties, RSC Adv. 3 (2013) 23737–23744.
[24] Y.C. Yang, Y. Liu, J.H. Wei, C.X. Pan, R. Xiong, J. Shi, Electrospun nanofibers of p-type $BiFeO_3$/n-type TiO_2 hetero-junctions with enhanced visible-light photocatalytic activity, RSC Adv. 4 (2014) 31941–31947.
[25] F. Qin, H.P. Zhao, G.F. Li, H. Yang, J. Li, R.M. Wang, Y.L. Liu, J.C. Hu, H.Z. Sun, R. Chen, Size-tunable fabrication of multifunctional Bi_2O_3 porous nanospheres for photocatalysis, bacteria inactivation and template-synthesis, Nanoscale 6 (2014) 5402–5409.
[26] J. Zhang, Q. Wang, L.H. Wang, X.A. Li, W. Huang, Layer-controllable WS_2-reduced graphene oxide hybrid nanosheets with high electrocatalytic activity for hydrogen evolution, Nanoscale 7 (2015) 10391–10397.
[27] S.Q. Liang, J. Zhou, J. Liu, A.Q. Pan, Y. Tang, T. Chen, G.Z. Fang, PVP-assisted synthesis of MoS_2 nanosheets with improved lithium storage properties, CrystEngComm 15 (2013) 4998–5002.
[28] U.A. Joshi, J.S. Jang, P.H. Borse, J.S. Lee, Microwave synthesis of single-crystalline perovskite $BiFeO_3$ nanocubes for photoelectrode and photocatalytic applications, Appl. Phys. Lett. 92 (2008) 242106.
[29] S. Li, Y.H. Lin, B.P. Zhang, Y. Wang, C.W. Nan, Controlled fabrication of $BiFeO_3$ uniform microcrystals and their magnetic and photocatalytic behaviors, J. Phys. Chem. C 114 (2010) 2903–2908.
[30] Y.L. Cheng, M. Zhang, G. Yao, L. Yang, J.J. Tao, Z.Z. Gong, G. He, Z.Q. Sun, Band gap manipulation of cerium doping TiO_2 nanopowders by hydrothermal method, J. Alloys Compd. 662 (2016) 179–184.
[31] S.G. Jeon, S.H. Park, J. Yu, J.Y. Song, Selective synthesis of nanospheres and nanosheets of bismuth subcarbonate, Chem. Lett. 44 (2015) 1717–1719.
[32] N.T.K. Thanh, N. Maclean, S. Mahiddine, Mechanisms of nucleation and growth of nanoparticles in solution, Chem. Rev. 114 (2014) 7610–7630.
[33] L.S. Zhong, J.S. Hu, H.P. Liang, A.M. Cao, W.G. Song, L.G. Wan, Self-assembled 3D flowerlike iron oxide nanostructures and their application in water treatment, Adv. Mater. 18 (2006) 2426–2431.
[34] F.D. Wang, V.N. Richards, S.P. Shields, W.E. Buhro, Kinetics and mechanisms of aggregative nanocrystal growth, Chem. Mater. 26 (2014) 5–21.
[35] Y.F. Yuan, S.M. Wood, K. He, W.T. Yao, D. Tompsett, J. Lu, A.M. Nie, M.S. Islam, R.S. Yassar, Atomistic insights into the oriented attachment of tunnel-based oxide nanostructures, ACS Nano 10 (2016) 539–548.
[36] Z.H. Wu, S.L. Yang, W. Wu, Shape control of inorganic nanoparticles from solution, Nanoscale 8 (2016) 1237–1259.
[37] Z. Chen, M.H. Cao, Synthesis, characterization, and hydrophobic properties of Bi_2S_3 hierarchical nanostructures, Mater. Res. Bull. 46 (2011) 555–562.
[38] J.W. Mullin, Crystallization, fourth ed., Butterworth Heinemann, Oxford, 2001.
[39] J.L. Yang, W.Z. Huang, Y.L. Cheng, C.J. Wang, Y. Zhao, L. Zhu, X.Q. Cao, Morphology-controlled synthesis of gadolinium fluoride nanocrystals via ultrasonic and salt assisted method, CrystEngComm 14 (2012) 899–907.